Mechatronics 49 (2018) 56–66

Contents lists available at ScienceDirect

Mechatronics

journal homepage: www.elsevier.com/locate/mechatronics

Design and adaptive balance control of a biped robot with fewer actuators for slope walking☆

Satoshi Ito*,[a], Shingo Nishio[b], Masaaki Ino[b], Ryosuke Morita[a], Kojiro Matsushita[a], Minoru Sasaki[a]

[a] Faculty of Engineering Gifu University, Japan
[b] Graduate School of Engineering Gifu University, Japan

ARTICLE INFO

Keywords:
Biped robot
DoF reduction
Hip joint structure
Slope adaptation
CoP feedback
Gravity compensation

ABSTRACT

Although reducing the number of actuators in mobile robots contributes to weight saving and results in high efficiency or damage reduction in the event of an accident such as falling over, ideally it should not degrade the robot's performance and functionality. In this study, we propose a new biped mechanism that reduces the number of actuators in a robot without sacrificing its ability to walk adaptively on slopes. We address two issues from both the mechanical and the control viewpoints that are required to achieve straight walking on slopes. For the biped mechanism, we studied the required degrees of freedom of the biped robot and then proposed an actuation mechanism for the hip joint structure. Subsequently, we designed and constructed a biped robot with six actuators, including two actuators for each ankle, no knees, and two actuators for the hip joint structure. For control, we applied feedback from the center of pressure (CoP) of the ground reaction forces in addition to gravity compensation and discussed the stability of CoP movement. Experiments conducted using the constructed biped robot with fewer actuators demonstrated the viability of the proposed mechanism in terms of walking on slopes and the effectiveness of the proposed control concept, which introduces adaptability to the biped robot.

1. Introduction

Biped robots have the advantage of simpler moving mechanisms than multi-legged robots, allowing us to decrease the number of independently movable joints, that is, the degrees of freedom (DoFs) of motion. The low-DoF mechanism, in other words, the mechanism with only a few actuators, is important for realizing biped robots. This mechanism allows us to reduce robot weight, which enhances the robot's walking efficiency and reduces the risk of damage in the event of a fall: if the robots are lightweight, the damage to instruments or humans around them, as well as to the robots themselves, is reduced.

Biped robots are essentially unstable systems. Their motion always involves the possibility of falling over. Thus, if a biped robot can adaptively maintain its balance, for example, even on a floor with an uneven gradient, then the areas where robots can be used would increase dramatically. However, such adaptability is generally accompanied by a variety of motions that normally require multiple DoFs. Thus, the challenge is to achieve adaptive locomotion with fewer actuators. To tackle this problem, mechanical design and control strategy should be considered in a complementary manner.

In this study, we attempt to design a biped mechanism with fewer actuators that can adaptively walk on a slope. The minimum DoF of a biped mechanism has already been discussed for various real-world situations [1], and a seven-DoF biped robot that can change direction was proposed [2]. Passive walking [3], which does not require actuators or power supplies, is another approach to achieving the goal of efficiency enhancement, that is, weight reduction due to a low DoF. Recently, an actuated dynamic walk based on passive walking [4,5] has been proposed. Although the gait in passive walking changes with the slope gradient via a simple mechanism, this adaptation is completely mechanical. A new concept for motor control accompanied by learning is required to achieve any kind of adaptation. For this control aspect, the most important concept is the zero-moment point (ZMP) [6,7]; To adapt to environmental changes, online planning of the center of mass (CoM) trajectory [8], footsteps [9], and angular momentum [10] is considered in combination with the ZMP criterion. Moreover, the center of pressure (CoP) is used to realize human-like walking [11]. Compliance control is an effective method [12] for locomotion in which the robot maintains contact with the ground. Environmental changes are sometimes treated as external force [13,14] or uneven terrain [15],

☆ This paper was recommended for publication by Associate Editor Prof Michael Ruderman.

* Corresponding author.
E-mail address: satoshi@gifu-u.ac.jp (S. Ito).

https://doi.org/10.1016/j.mechatronics.2017.11.007
Received 27 March 2017; Received in revised form 18 October 2017; Accepted 11 November 2017

where the robot's behaviors are evaluated under the modeled conditions. By performing a robot demonstration and mathematical analysis, some studies have aimed to ensure stability of the control result by means of linearized analysis [16], return (Poincaré) maps [17,18] and nonlinear dynamics [19]. Our approach is different in that we aim to ensure stability of the body balance based on CoP feedback.

By limiting the problem to straight walking on a constant slope, in this study, we address two issues: (1) a mechanism of biped robots with a small number of actuators from the mechanical viewpoint and (2) the achievement of adaptive behavior from the control viewpoint. Moreover, in this study, we propose a new hip joint mechanism that achieves not only alternative leg swings but also lateral sway while keeping the two legs parallel, and a control method that adapts a six-DoF robot to unknown external forces by adjusting the posture, resulting in adaptive biped walking on a slope. In Section 2, we discuss the DoFs required to achieve slope locomotion and present a novel design for the hip joint with fewer actuators [20]. Next, in Section 3, we introduce a balance control method to adapt to changes in the slope gradient. We have already proposed a control scheme based on CoP feedback [21]. To improve the response speed, we introduced gravity compensation [22]. In this study, we present a scheme to achieve stability based on CoP feedback control with gravity compensation by proving the controllability of a linearized system in the stationary state because the control law is basically constructed as the state feedback of that linearized system. Section 4 is devoted to robot experiments, and Section 5 concludes the paper.

2. Design of a biped robot with a small number of actuators

2.1. Minimal DoF consideration

The target behavior of our biped robot is straight walking on a constant slope of unknown gradient. First, we discuss the required number of DoFs that will allow the biped robot to walk on a uniform slope.

Biped robots move by repeating support leg exchanges between their right and left legs. To adapt to a slope in a single-support phase, an ankle joint needs to have two DoFs: pitch and roll. Here yaw rotation is not considered.

While walking, both legs are swung alternately in the anterior-posterior direction. This motion can be executed with one DoF if the legs are swung symmetrically within the sagittal plane. Simultaneously, the weight of the robot must be moved in the lateral direction to switch the support leg before lifting and swinging the other leg. Introducing a constraint that the legs must be parallel to each other, which can be achieved with one DoF, means that the ankle joints must then move in a coordinated manner. Mechanically integrating these types of sagittal and frontal plane movements at the hip joint structure limits the number of required DoFs to two.

In summary, a bipedal robot with six DoFs, with two in each of the ankles and two in the hip joint structure, will be able to adaptively walk on a regular slope.

2.2. New reduced DoF structure for the hip joint

The key to the above ideas about a robot with a reduced number of DoFs is the realization of a hip joint structure that allows simultaneous alternate leg swing and lateral sway.

Initially, let us consider the mechanism for alternate leg swing in the anterior-posterior direction. To realize this motion, we introduced differential gear functions, which are shown on the left in Fig. 1. Assuming that the leg segments are fixed to each side gear, if a central pinion gear drives the two side gears, the side gear deviates equally in the opposite direction. Thus, oscillation of the central gear leads to alternate leg swing back and forth on both sides.

Lateral sway requires a gap between the two legs to prevent them from interfering with each other. A large central gear can be used to create this wide gap, but large gears are generally heavy. Therefore, we synchronized the function of the central gear with two coupled gears that are connected mechanically, for example, by a timing belt, as shown on the right in Fig. 1.

To achieve lateral sway, we introduced U-shaped bases, as shown on the right in Fig. 1. The leg segment was fixed to the side-beveled gear in the base. Each U-shaped base can achieve roll rotations, but these rotations do not block the leg swing in the anterior-posterior direction. While coupling the roll rotations of two U-shaped bases, for example, by using a timing belt, as shown in Fig. 2, the two legs were always maintained parallel to each other. This constraint resulted in lateral sway when the legs contacted the ground. To achieve roll rotation coupling, another axis was added in the opposite direction to support the U-shaped base, sharing the rotation axis for the leg-swing motion. This sharing of the rotation axis not only allowed rotation of the two synchronized central gears without interference but also distributed the body weight across the two axes at the back and front.

Because of these mechanisms, the robot can lift the leg opposite to the body slant and then swing this leg while keeping it parallel to the other leg in the front view.

2.3. Robot construction

Fig. 3 shows the biped robot that we constructed, which contains the hip joint structure described in this section. Its dimensions are as follows: height = 290 mm, width = 270 mm, and weight = 4.12 kg (with six servo motors). Its feet measured 160 mm in length.

After devising the hip joint structure, we focused on the motor configuration to prevent mechanical interference between the robot's links. Two motors were installed on this hip joint structure for its actuation to balance the robot's weight symmetrically. Timing belts were used to transmit the driving force from the motor axis to the hip joint

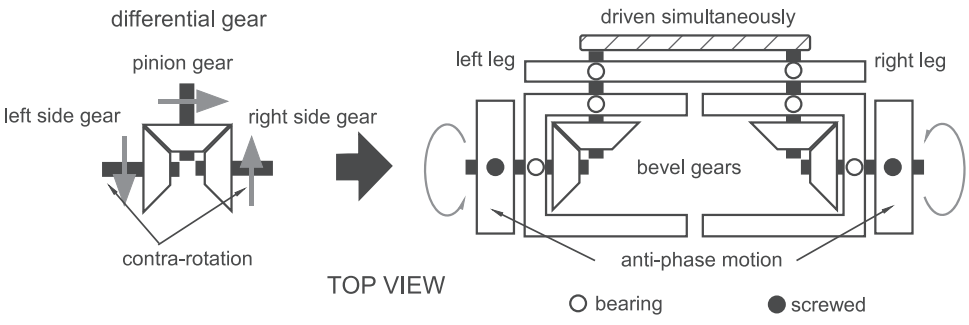

Fig. 1. Leg-swing mechanism.

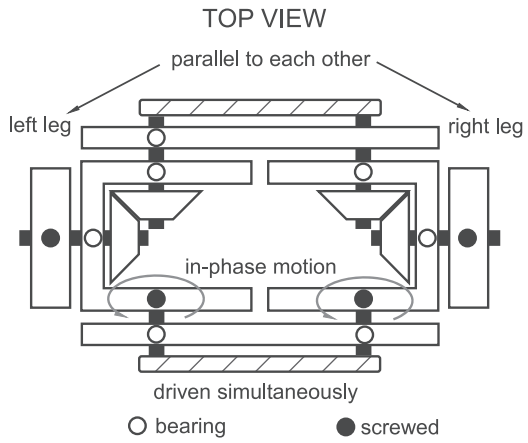

Fig. 2. Reduced-DoF mechanism for lateral motion.

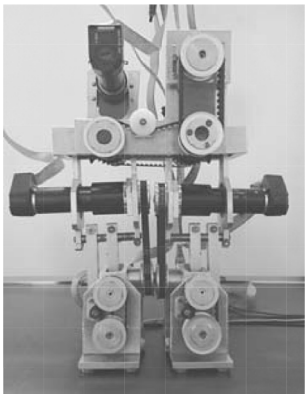

Fig. 3. Overview of the biped robot.

DoFs, whose tension reduced the backlash between pulleys attached at the motor and hip joint axes.

The sagittal DoFs of the ankle joint were actuated by the motor placed in the middle of the leg, whereas the frontal ones were driven by the motor in the foot segment.

The same motors (Maxon RE25) were used for the actuation of all DoFs; the reduction gear ratios differed among the hip joints (111:1), ankle pitch (28:1), and roll rotations (66:1).

3. Biped control based on CoP feedback

3.1. Concept

The key to realizing biped control is the ZMP-based method. The motion represented by the positional trajectory of joint angles or the CoM of a few links was planned initially to ensure that the ZMP calculated using the gravitational and inertial forces remained inside the support polygon, which is the convex hull that includes all contact points with the ground. Then, positional feedback control was applied to track this trajectory. This ensured zero turnover of the robot in the sense that the foot segment remained steady without rotating around its edge. This method is quite powerful and effective; however, it does not monitor the actual ZMP position, which does not always remain within the support polygon if the parameters of the robot's environment, such as the gradient of the ground, change.

To deal with environmental variations, additional information should be added to the control law. For example, we focused on the

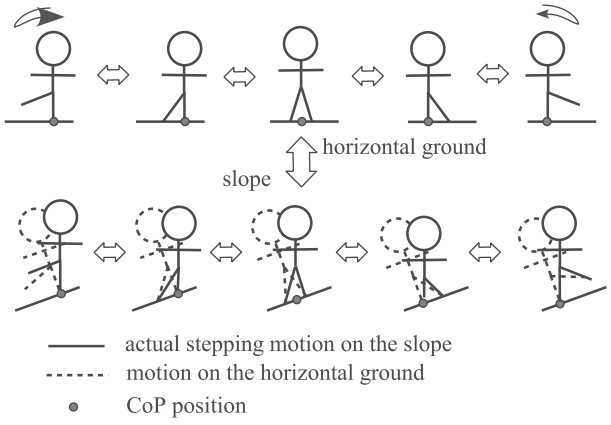

Fig. 4. CoP trajectory on flat and sloped ground.

ground reaction forces [21]. In fact, the ZMP is equivalent to the CoP of the ground reaction forces [23], which means that the ground reaction forces contain useful information regarding balance. According to our idea for adapting to environmental changes, although the joints or CoM trajectories vary with the slope angles, the trajectory of the CoP position does not change during locomotion, especially in the lateral direction, as illustrated in Fig. 4. Because of this invariance, we chose the CoP trajectory as the control reference. We proposed a balance control law demonstrating the maintenance of adaptive balance during static standing [21] and in-place stepping [24]. However, biped walking has not been realized yet owing to slow response to desired trajectories. The control law described in the following sections improves upon this aspect by adding gravity compensation, as already proposed in a few papers [25,26].

3.2. CoP control in the double-support phase

3.2.1. Control law

Static balance retention based on CoP feedback along with gravity compensation was proposed, and its effect was investigated in our previous work [27]. Here, we extend this concept to CoP tracking control in the double-support phase. Gravity compensation is introduced into the control scheme without gravity compensation in [24] to hasten the response.

In the double-support phase, the CoP position moves from beneath the support leg in the previous single-support phase to the other leg. This type of CoP movement is realized by using the desired trajectory of the $P_d = P_d(t) \in \mathscr{R}$, which sets the desired position as time variant according to the stability of the CoP feedback control.

However, in the biped double-support phase, a closed-link structure is constructed. To describe this action, we consider a non-vertical constraint path of the CoM for the entire biped robot; a new coordinate frame is defined whose variable is denoted by $\phi \in \mathscr{R}$. Here, let us assume that ϕ uniquely determines all joint angles $\theta \in \mathscr{R}^n$ of the biped robot ($n = 4$ for the robot constructed in Section 2; see Appendix A and Appendix B). Then, the deviation of ϕ uniquely defines the amount of deviation of all the joint angles θ based on the Jacobian matrix $J(\theta) \in \mathscr{R}^{n\times 1}$, according to

$$\Delta\theta = J(\theta)\cdot\Delta\phi. \tag{1}$$

Now, we define the control law. First, we calculate the generalized torque $\tau_\phi \in \mathscr{R}$ in the coordinate frame ϕ which requires CoP tracking to $P_d(t)$.

$$\tau_\phi = -K_d\dot{\phi} + K_p(\phi_d - \phi) + K_{CoP}\int (P_d - P_{CoP})dt + G(\theta, g), \tag{2}$$

where $G(\theta, g)$ is the gravity term in the coordinate frame ϕ. The following equation holds based on the virtual work principle:

$$\tau_\phi = J(\theta)^T \tau, \tag{3}$$

where τ denotes a generalized force, which is a joint torque vector, corresponding to the joint angle θ. Finally, we obtain all joint torques using $(J^T(\theta))^*$, which is the generalized inverse matrix of $J^T(\theta)$ and is given by

$$\tau = (J^T(\theta))^* \tau_\phi. \tag{4}$$

Because the double-support phase with the large support polygon facilitates balance retention in comparison with the single-support phase, the control law may not necessarily require the gravity compensation term. Analysis without the gravity compensation term has already been conducted in our previous study [24].

3.2.2. Stationary state

Now, we assume that the robot dynamics has been restricted to the one-dimensional path ϕ so as to the double-support phase of our robot constructed in Section 2. Its dynamics is described by

$$M(\theta)\ddot{\phi} + C(\theta, \dot{\theta}) + G(\theta, g) + \xi(\theta, \mathbf{F}_e) = \tau_\phi. \tag{5}$$

Here, $M(\theta) \in \mathscr{R}$ is an inertia term, $C(\theta, \dot{\theta}) \in \mathscr{R}$ is a Coriolis-centrifugal force, $G(\theta, g) \in \mathscr{R}$ is the gravitational force, and $\xi(\theta, \mathbf{F}_e) \in \mathscr{R}$ is the effect of an external force $\mathbf{F}_e \in \mathscr{R}^2$ exerted on the robot's CoM. The derivation is given in the Appendix C. In addition, according to the equations in the Appendix D, the CoP position is given as

$$P_{CoP} = P(\theta)\tau_\phi + Q(\theta, \dot{\theta}) + R(\theta, g, \mathbf{F}_e), \tag{6}$$

where $P(\theta) \in \mathscr{R}$ denotes the effect of τ_ϕ on the CoP position, $Q(\theta, \dot{\theta}) \in \mathscr{R}$ represents the effect of the Coriolis-centrifugal force, and $R(\theta, g, \mathbf{F}_e) \in \mathscr{R}$ represents the effects of gravity and external force. Then, control law (2) is applied to these equations.

By introducing a new state variable $\tau_{CoP} \in \mathscr{R}$, which is defined as

$$\tau_{CoP} = \int (P_d - P_{CoP})dt, \tag{7}$$

we obtain the new dynamics,

$$\dot{\tau}_{CoP} = P_d - P_{CoP}, \tag{8}$$

and the state variables are defined as $\mathbf{x} = [\phi \;\; \dot{\phi} \;\; \tau_{CoP}]^T \in \mathscr{R}^3$. The stationary state $\bar{\mathbf{x}} = [\bar{\phi} \;\; 0 \;\; \bar{\tau}_{CoP}]^T$, that is, the equilibrium point, is obtained by solving $\dot{\mathbf{x}} = \mathbf{0}$. Specifically, from (8), $P_{CoP} = P_d$ holds in the stationary state. Moreover, the control law takes the stationary value, $\bar{\tau}_\phi = K_p(\phi_d - \bar{\phi}) + K_{CoP}\bar{\tau}_{CoP} + G(\bar{\theta}, g)$.

3.2.3. Local stability

Next, to examine the local stability of the stationary state $\bar{\mathbf{x}}$, we linearize (5) and (8) using (6) around the stationary state $\bar{\mathbf{x}}$. Namely, we obtain the dynamics of the error $\Delta\mathbf{x} = [\Delta\phi \;\; \Delta\dot{\phi} \;\; \Delta\tau_{CoP}]^T$ by using $\mathbf{x} = \bar{\mathbf{x}} + \Delta\mathbf{x}$. Note that the control input can be written as follows:

$$\tau_\phi = \bar{\tau}_\phi + \Delta\tau_\phi, \tag{9}$$

$$\Delta\tau_\phi = -K_d\Delta\dot{\phi} - K_p\Delta\phi - K_{CoP}\Delta\tau_{CoP} = -K\Delta\mathbf{x}, \tag{10}$$

$$K = [K_p \;\; K_d \;\; K_{CoP}]^T. \tag{11}$$

Replacing $\Delta\tau_\phi$ with u, the error dynamics becomes

$$\Delta\dot{\mathbf{x}} = A\Delta\mathbf{x} + Bu, \tag{12}$$

where

$$A = \begin{bmatrix} 0 & 1 & 0 \\ -\bar{\xi}'\bar{J}/\bar{M} & 0 & 0 \\ (\bar{P}'\bar{\tau}_\phi + \bar{P}\bar{G}' + \bar{R}')\bar{J} & 0 & 0 \end{bmatrix}, \tag{13}$$

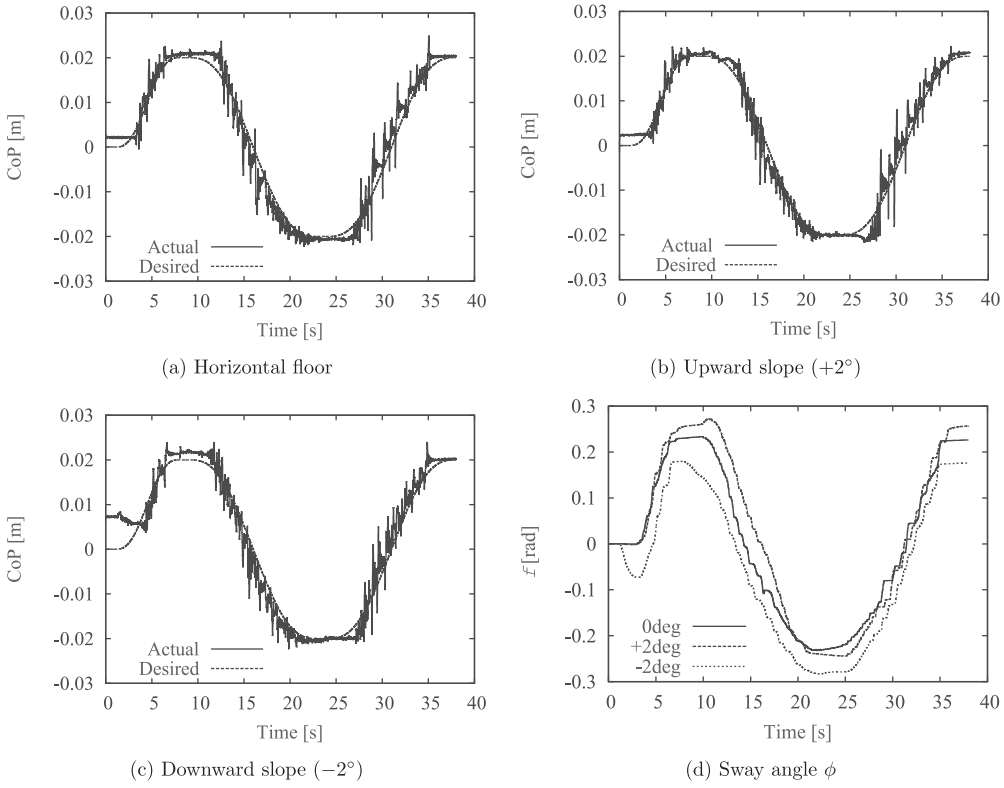

Fig. 5. Experiments of CoP tracking in the double-support phase where the right foot is placed forward.

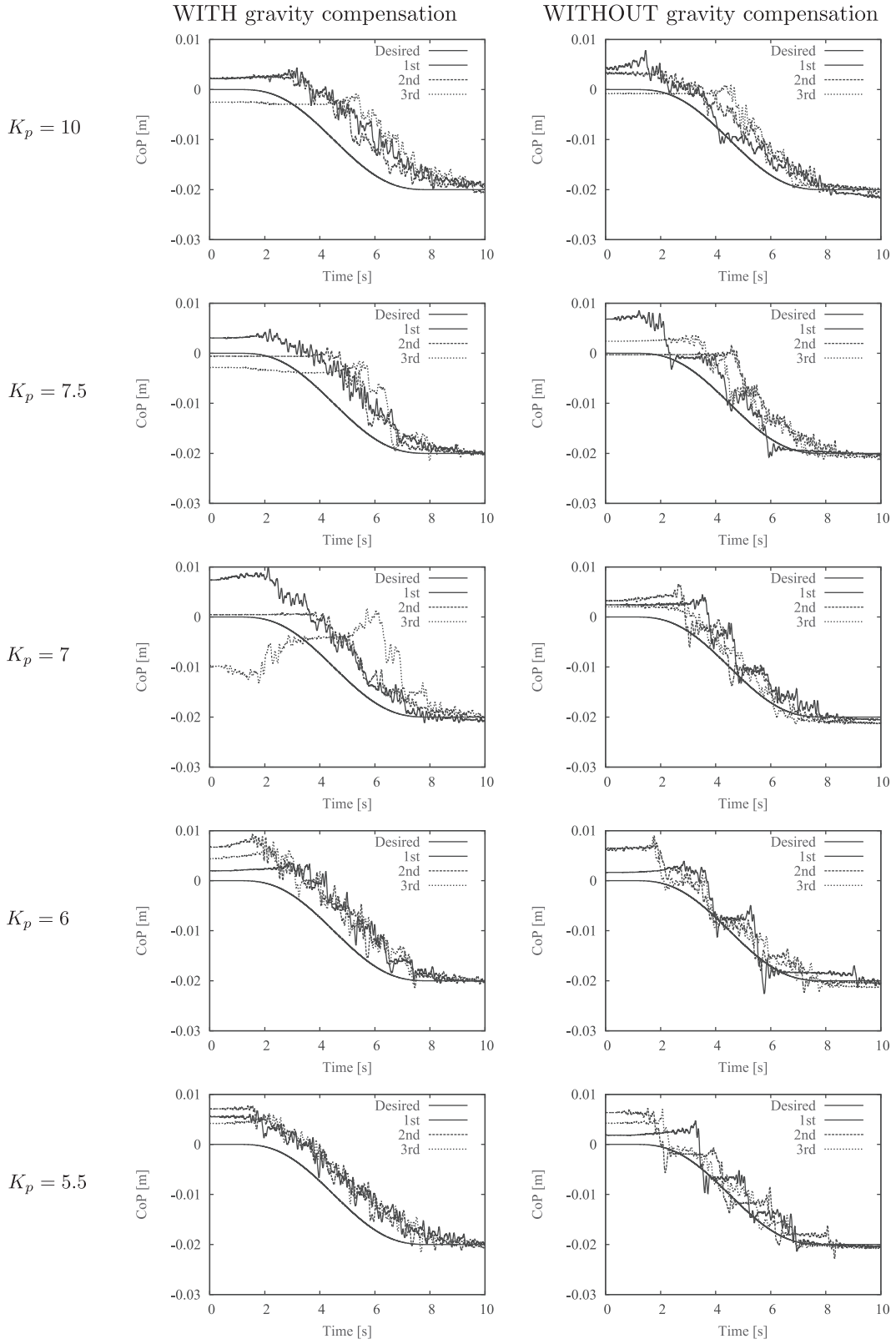

Fig. 6. Comparison of control laws with and without gravity compensation.

$$B = \begin{bmatrix} 0 \\ 1/\overline{M} \\ \overline{P} \end{bmatrix}. \tag{14}$$

Here, $\bar{\cdot}$ denotes the stationary state and $'$ denotes the derivation with respect to θ. Namely, $\overline{J} = J(\bar{\theta}) \in \mathscr{R}^n$, $\overline{M} = M(\bar{\theta}) \in \mathscr{R}$, $\overline{G} = G(\bar{\theta}, g) \in \mathscr{R}$, $\overline{\xi} = \xi(\bar{\theta}, \mathbf{F}_e) \in \mathscr{R}$, $\overline{P} = P(\bar{\theta}) \in \mathscr{R}$, $\overline{R} = R(\bar{\theta}, g, \mathbf{F}_e) \in \mathscr{R}$, $\overline{G}' = \frac{\partial}{\partial\theta} G(\bar{\theta}, g) \in \mathscr{R}^{1\times n}$, $\overline{\xi}' = \frac{\partial}{\partial\theta}\xi(\bar{\theta}, g) \in \mathscr{R}^{1\times n}$, $\overline{P}' = \frac{\partial}{\partial\theta} P(\bar{\theta}) \in \mathscr{R}^{1\times n}$, $\overline{R}' = \frac{\partial}{\partial\theta} R(\bar{\theta}, g, \mathbf{F}_e) \in \mathscr{R}^{1\times n}$ and

$$\overline{\tau}_\phi = \overline{G} + \overline{\xi}. \tag{15}$$

The determinant of this controllability matrix Δ_c becomes

$$\Delta_c = \begin{vmatrix} 0 & 1/\overline{M} & 0 \\ 1/\overline{M} & 0 & -\overline{\xi}'\overline{J}/\overline{M}^2 \\ \overline{P} & 0 & (\overline{P}'\overline{\tau}_\phi + \overline{P}\overline{G}' + \overline{R}')\overline{J}/\overline{M} \end{vmatrix}$$
$$= -(\overline{P}\overline{\xi}' + \overline{P}'\overline{\tau}_\phi + \overline{P}\overline{G}' + \overline{R}')\overline{J}/\overline{M}^3$$
$$= -\frac{1}{\overline{M}^3}\cdot\frac{\partial}{\partial\phi}(\overline{P}\overline{\tau}_\phi + \overline{R})\Big|_{\mathbf{x}=\overline{\mathbf{x}}} = -\frac{1}{\overline{M}^3}\cdot\frac{\partial}{\partial\phi}P_{CoP}\Big|_{\mathbf{x}=\overline{\mathbf{x}}}. \quad (16)$$

Here, $\frac{\partial}{\partial\phi}P_{CoP}\Big|_{\mathbf{x}=\overline{\mathbf{x}}}$ denotes deviation of the CoP when the CoM moves along the one-dimensional path ϕ. This term is supposed to be nonzero because ϕ is assumed to be non-vertical, which leads to certain CoP deviations. Accordingly, the controllability matrix has full rank, and thus the linearized system (12) is controllable.

If the linear system is controllable, the state feedback $u = -K\Delta\mathbf{x}$ sets the eigenvalues of dynamics (12) arbitrarily by selecting the coefficient matrix K. Now, u is being defined as $-K\Delta\mathbf{x}$ because it replaces $\Delta\tau_\phi$ given by (10). In conclusion, the stationary state $\overline{\mathbf{x}}$ is stabilized by selecting K suitably, for example, based on the framework of optimal control. Although P_d will be time-variant in reality, this local stability allows the CoP to follow it.

4. Robot experiments

4.1. Setups

The goal of the experiments was to confirm the following two points: (1) walking ability of the small-DoF robot designed and constructed in Section 2 and (2) effectiveness of the balance control with the CoP feedback proposed in Section 3 for slope walking with adaptation to the gradient.

To detect the vertical components of the ground reaction forces, load cells (KYOWA LMA-A-50N-P) were attached to each corner of the robot's square soles; in total, eight load cells were attached. The value of strain was translated into electrical data and acquired using an analog-to-digital converter board after amplification. In addition, the joint angles of the robot were detected using optical encoders that were included with each motor, and their pulses were counted using counter boards. These data were processed using a personal computer running a real-time operating system, and the motor commands corresponding to the joint torque were output from a digital-to-analog converter board. Motor drivers received this command and supplied the electric current required to a direct current servo motor.

4.2. CoP tracking in the double-support phase

To confirm CoP tracking in the double-support phase, the initial state of the robot was set such that its right foot was placed 4 cm ahead of its left foot. The desired CoP trajectory was set to sway 4 cm laterally in 14 s from left to right to left again. Feedback gains were set as $K_d = 0.0005$, $K_p = 15$, and $K_{CoP} = 300$. The control scheme started 2 s after the start of the experiments. Three scenarios, horizontal floor, 2° upward slope, and − 2° downward slope, were tested under the same conditions, that is, no changes in the controller.

The time courses of the CoP are shown along with its desired trajectories in Fig. 5(a)–(c) for each condition. Independent of the slope angle, similar trajectories were obtained under the three different scenarios. This indicates that balance control based on CoP tracking along with gravity compensation was not affected by environmental conditions represented by external forces such as change in the gravity direction on the slope, as shown in Fig. 4. Fig. 5(d) shows the time course of the approximate value of the lateral sway angle ϕ with respect to the normal direction of the slope. This result implies that the posture in the lateral sway is adjusted automatically with the slope angle.

Next, to demonstrate the effect of the gravity compensation term, experiments with and without this term were conducted for a simple lateral movement on a horizontal floor. The biped robot was made to stand upright at first, and the desired CoP position was moved from the center (0 m) to 0.02 m toward the left (− 0.02 m) in 5 s at 2 s after the start of the experiments. The feedback gains were set as $K_d = 0.0005$ and $K_{CoP} = 75$ with several K_p values of 10, 7.5, 7, 6, and 5.5. Because the first experiment showed a noisy CoP trajectory, a 5 Hz low-pass filter was applied for the detection of the ground reaction forces. Three experiments were conducted for each condition.

The time courses of the CoP trajectories are shown in Fig. 6. For the same K_p value, rapid responses can be observed for the control law without gravity compensation: this is because gravity comüÊpensation is exerted to maintain the upright posture, and thus it does not facilitate the movement of CoP. For the same reason, improved responses are obtained for the smaller K_p values. However, these K_p values degrade the stability of the response. The responses tend to oscillate for small K_p values without gravity compensation. These facts imply that if K_p is constant, larger feedback gains can be set to K_{CoP} of the control law with gravity compensation than those for the control law without it. Because K_{CoP} controls convergence of the CoP to its desired value, gravity compensation improves the CoP response by combining the larger K_{CoP}. In fact, in the experiment in Fig. 5, which shows rapid tracking, K_{CoP} was set to 300.

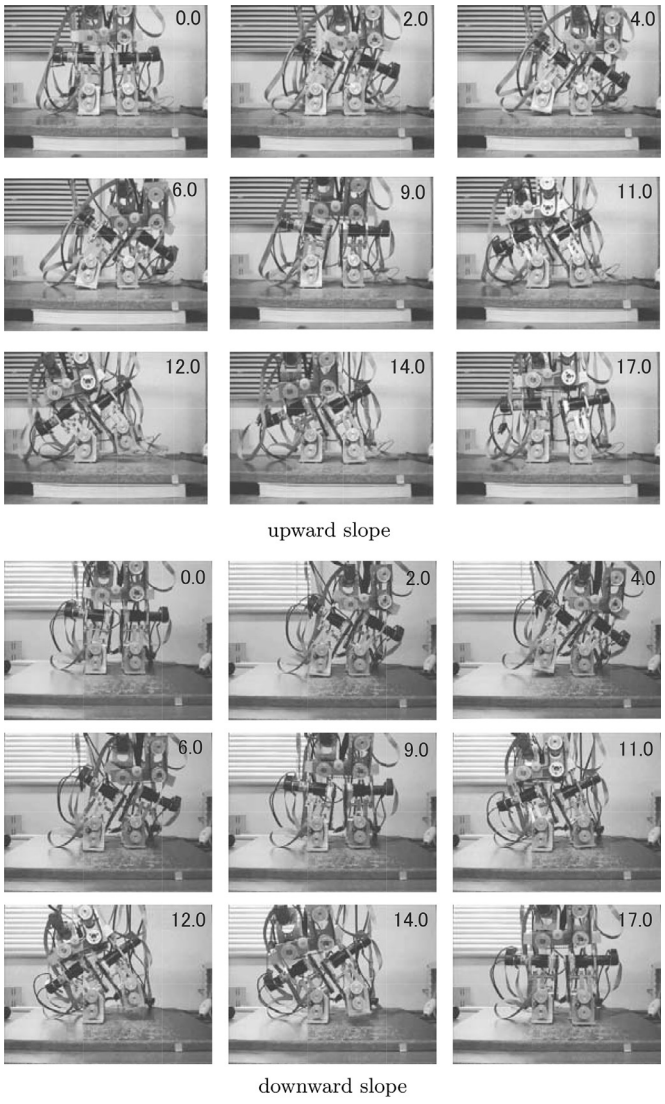

Fig. 7. Photos of a biped walk on a slope.

4.3. Biped walking

We walked our biped robot on 5° upward and downward slopes. The control law based on the CoP feedback concept was used for balance control during this experiment. Even though the controller was not different, that is, the reference trajectory of the CoP and the feedback gains were the same, the robot could walk on two slopes with different gradients [22]. Photos of the slope walking experiment are shown in Fig. 7.

These experiments demonstrate that a robot with a small-DoF hip structure can accomplish slope walking and that the control strategy based on the CoP feedback shown in Fig. 4 works effectively.

5. Conclusion

To reduce the number of actuators for reducing robot weight, we proposed a method for reducing the number of DoFs of a biped robot without affecting its adaptability. For maintaining adaptability, we focused on changes in the ground's gradient, and the target motion of the robot was to achieve straight walking on flat slopes of unknown gradient. To achieve adaptive walking on slopes with a small-DoF robot, a few challenges needed to be addressed from the mechanical and control perspectives.

From the mechanical viewpoint, we first discussed the minimum number of DoFs of the leg structure. On the basis of this discussion, we constructed a six-DoF biped robot with two DoFs for each ankle, no knees, and two DoFs for the hip joint structure. From the control viewpoint, CoP feedback was applied because joint angles are usually affected by environmental changes, whereas the CoP trajectory remains invariant. Considering the CoP shift in the double-support phase as an example, the stability of CoP movement was discussed.

The experiments with the small-DoF biped robot that we constructed showed adaptive postural changes during CoP movements in the double-support phase, which indicated the effectiveness and stability of the control law proposed herein. In addition, biped walking on both the 5° upward and downward slopes was realized. The experiments demonstrated that a biped mechanism with a small DoF helps a robot to walk on slopes. Neither the control law nor the reference needed to be adjusted even if a disturbance, including external forces due to environmental changes, occurs unexpectedly. However, this robot walks only in a straight line, and its range of motion should be extended. Further work is required to this end, including the addition of yaw rotation to turn the robot and increasing the speed of robot motion from the mechanical and control viewpoints.

Acknowledgments

The authors would like to thank Mr. Akihiro Nakazawa, Mr. Takeshi Onozawa, and Mr. Kazuki Yajima for their assistance with the robot experiments. This study was partly supported by a grant from the Japan Science and Technology Agency (2009 Seeds-A, No. 789).

Appendix A. Double-support model within a lateral plane

First, the symbols used in this paper are summarized in Tables 1 and 2.

Assuming that the feet always maintain contact with the ground, the biped robot constructed in Section 2 possesses one DoF in the double-support phase; its dynamic behavior can be described approximately by using the five-link model, as shown in Fig. A1.

In this mode, the following assumptions are made. Only motion within the frontal plane is considered. The five-link model consists of one body, two legs, and two feet within a two-dimensional plane. Here, the ankle joints are located at the center of the foot at the same height as the ground. The feet never slip on the ground. At both ends, the feet are in contact with the ground, and their vertical components F_{RO}, F_{RI}, F_{LO}, and F_{LI}, are measurable. In addition, all joints in the ankle and hip can produce joint torque $\mathbf{T}$ and their deviations θ and velocities $\dot{\theta}$ are detectable, where each subscript denotes the right ankle, right hip, left hip, and left ankle, respectively.

To express environmental changes, a constant external force $\mathbf{F}_e$ is assumed to be exerted on the CoM position (x_G, y_G). Here, the origin is set at the midpoint between the two ankle joints.

Table 1
List of symbols (part 1).

Symbol	Explanation
P	CoP position
P_d	Desired value of CoP position
ϕ	Lateral sway angle of robot in sagittal model
θ_{RA}	Angle deviation at right ankle joint
θ_{RH}	Angle deviation at right hip joint
θ_{LH}	Angle deviation at left hip joint
θ_{LA}	Angle deviation at left ankle joint
θ_L	Sway angle of left leg
θ_R	Sway angle of right leg
ℓ	Length from ground to CoM of leg
ℓ_B	Half-length of body
L	Leg ength
x_f	Distance from origin of coordinate frame to ankle joint
(x_R, y_R)	CoM position of right leg
(x_L, y_L)	CoM position of left leg
(x_B, y_B)	CoM position of body
θ_B	Sway angle of body
m_B	Mass of body
m_L	Mass of leg (same on both sides)
I_B	Moment of inertia of body
I_L	Moment of inertia of leg (same on both sides)
K_d	Feedback gain of $\dot{\phi}$ for τ_ϕ in (2)
K_p	Feedback gain of ϕ for τ_ϕ in (2)
K_{CoP}	Feedback gain of CoP position P for τ_ϕ in (2)

Table 2
List of symbols (part 2).

Symbol	Explanation
τ_{CoP}	Integrated error of CoP from desired position (Eq. (7))
τ_{ϕ}	Generalized torque with respect to generalized coordinate ϕ
τ_{RA}	Torque at right ankle joint
τ_{RH}	Torque at right hip joint
τ_{LH}	Torque at left hip joint
τ_{LA}	Torque at left ankle joint
F_x^{LH}	Horizontal component of interaction force at left hip joint
F_y^{LH}	Vertical component of interaction force at left hip joint
F_x^{RH}	Horizontal component of interaction force at right hip joint
F_y^{RH}	Vertical component of interaction force at right hip joint
F_x^{LA}	Horizontal component of interaction force at left ankle joint
F_y^{LA}	Vertical component of interaction force at left ankle joint
F_x^{RA}	Horizontal component of interaction force at right ankle joint
F_y^{RA}	Vertical component of interaction force at right ankle joint
F_{RO}	Vertical component of ground reaction force outside of right foot
F_{RI}	Vertical component of ground reaction force inside of right foot
F_{LO}	Vertical component of ground reaction force outside of left foot
F_{LI}	Vertical component of ground reaction force inside of left foot
F_x	Horizontal component of external force in sagittal model
F_y	Vertical component of external force in sagittal model

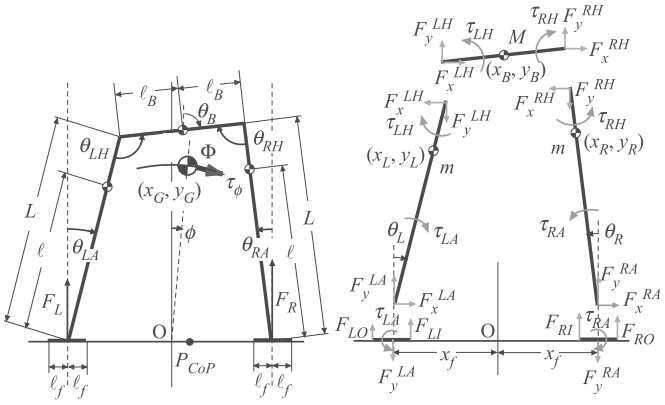

Fig. A1. Notation for derivation of the motion equation.

Appendix B. Definition of the coordinate ϕ

The lateral motion of this five-link model has only one DoF: sway angle ϕ, a new coordinate frame expressing the CoM position that uniquely determines each joint angle θ in the range $0 < \theta_{RH} < \pi$, $0 < \theta_{LH} < \pi$. We define ϕ as

$$\phi = \arctan \frac{x_G}{y_G}. \tag{B.1}$$

Here, x_G and y_G are described by

$$x_G = 2\rho \cos \frac{\theta_{RA} + \theta_{LA}}{2} \sin \frac{\theta_{LA} - \theta_{RA}}{2}, \tag{B.2}$$

$$y_G = 2\rho \cos \frac{\theta_{RA} + \theta_{LA}}{2} \cos \frac{\theta_{LA} - \theta_{RA}}{2}, \tag{B.3}$$

where

$$\rho = \frac{m_B L + 2m_L \ell}{2(m_B + 2m_L)}. \tag{B.4}$$

From this definition, we derived the Jacobian matrix in (1). Using (B.2) and (B.3), we obtain

$$\frac{x_G}{y_G} = \tan \frac{\theta_{LA} - \theta_{RA}}{2}. \tag{B.5}$$

Substituting the above equation into (B.1), we obtain

$$\dot{\phi} = \frac{\dot{\theta}_{LA} - \dot{\theta}_{RA}}{2}. \tag{B.6}$$

Conversely, the kinematic relationship between the joint angles is given by

$$-\theta_{RA} + \theta_{RH} + \theta_{LH} - \theta_{LA} = \pi. \tag{B.7}$$

Differentiating this equation, we obtain

$$-\dot{\theta}_{RA} + \dot{\theta}_{RH} + \dot{\theta}_{LH} - \dot{\theta}_{LA} = 0. \tag{B.8}$$

In addition, the CoM position of the body link located at its midpoint, (x_B, y_B), can be described in two ways:

$$\begin{bmatrix} x_B \\ y_B \end{bmatrix} = \begin{bmatrix} -x_f + L\sin\theta_{RA} + \ell_B \sin(\theta_{LH} - \theta_{LA}) \\ L\cos\theta_{RA} + \ell_B \cos(\theta_{LH} - \theta_{LA}) \end{bmatrix} = \begin{bmatrix} x_f - L\sin\theta_{LA} - \ell_B \sin(\theta_{LH} - \theta_{LA}) \\ L\cos\theta_{LA} - \ell_B \cos(\theta_{LH} - \theta_{LA}) \end{bmatrix}. \tag{B.9}$$

On differentiating the above expressions, the following equations hold:

$$\begin{bmatrix} L\dot{\theta}_{RA}\cos\theta_{RA} + \ell_B(\dot{\theta}_{LH} - \dot{\theta}_{LA})\cos(\theta_{LH} - \theta_{LA}) \\ -L\dot{\theta}_{RA}\sin\theta_{RA} - \ell_B(\dot{\theta}_{LH} - \dot{\theta}_{LA})\sin(\theta_{LH} - \theta_{LA}) \end{bmatrix} = \begin{bmatrix} -L\dot{\theta}_{LA}\cos\theta_{LA} - \ell_B(\dot{\theta}_{LH} - \dot{\theta}_{LA})\cos(\theta_{LH} - \theta_{LA}) \\ -L\dot{\theta}_{LA}\sin\theta_{LA} + \ell_B(\dot{\theta}_{LH} - \dot{\theta}_{LA})\sin(\theta_{LH} - \theta_{LA}) \end{bmatrix}. \tag{B.10}$$

Solving the three Eqs. (B.6), (B.8), and (B.10) with four variables $\dot{\theta}$, the relationship between $\dot{\theta}$ and $\dot{\phi}$ is represented by

$$\dot{\theta} = \frac{2}{J_1 + J_3}\begin{bmatrix} -J_1 \\ -J_1 + J_2 \\ J_3 - J_2 \\ J_3 \end{bmatrix}\dot{\phi} = \mathbf{J}(\theta)\dot{\phi}, \tag{B.11}$$

$$J_1 = 2\ell_B \sin\theta_{LH}, \tag{B.12}$$

$$J_2 = L\sin(\theta_{LH} + \theta_{RH}), \tag{B.13}$$

$$J_3 = 2\ell_B \sin\theta_{RH}. \tag{B.14}$$

Now, we can obtain the Jacobian matrix in (1).

Appendix C. Motion equations

The equation of motion with respect to ϕ is obtained as follows:

$$M(\theta)\ddot{\phi} + C(\theta, \dot{\theta}) + G(\theta, g) + \xi(\theta, \mathbf{F}_e) = \tau_\phi. \tag{C.1}$$

Below, we derive this equation.

Then, ϕ is described using $\mathbf{X} \in \mathscr{R}^9$ as

$$\phi = J_{\phi 1}\theta = J_{\phi 2}\mathbf{X}, \tag{C.2}$$

$$\theta = J_\theta \mathbf{X}, \tag{C.3}$$

where

$$J_{\phi 1} = \begin{bmatrix} -\frac{1}{2} & 0 & 0 & \frac{1}{2} \end{bmatrix} \in \mathscr{R}^{1\times 4}, \tag{C.4}$$

$$J_{\phi 2} = \begin{bmatrix} 0 & 0 & 0 & 0 & 0 & \frac{1}{2} & 0 & 0 & -\frac{1}{2} \end{bmatrix} \in \mathscr{R}^{1\times 9}, \tag{C.5}$$

$$J_\theta = \begin{bmatrix} 0 & 0 & 0 & 0 & 0 & 0 & 0 & 0 & 1 \\ 0 & 0 & 1 & 0 & 0 & 0 & 0 & 0 & 1 \\ 0 & 0 & -1 & 0 & 0 & 1 & 0 & 0 & 0 \\ 0 & 0 & 0 & 0 & 0 & 1 & 0 & 0 & 0 \end{bmatrix} \in \mathscr{R}^{4\times 9}. \tag{C.6}$$

The kinematic constraints of the link mechanism are written as

$$C_C(\mathbf{X}) = 0, \tag{C.7}$$

where

$$C_C(\mathbf{X}) = \begin{bmatrix} x_B - \ell_B \sin\theta_B - x_L - \ell_s \sin\theta_L \\ y_B - \ell_B \cos\theta_B - y_L - \ell_s \cos\theta_L \\ x_B + \ell_B \sin\theta_B - x_R + \ell_s \sin\theta_R \\ y_B + \ell_B \cos\theta_B - y_R - \ell_s \cos\theta_R \\ x_L - \ell \sin\theta_L \\ y_L - \ell \cos\theta_L \\ x_R + \ell \sin\theta_R \\ y_R - \ell \cos\theta_R \end{bmatrix} \in \mathscr{R}^8, \tag{C.8}$$

$$\ell_s = L - \ell. \tag{C.9}$$

The motion equation is expressed as

$$M\ddot{\mathbf{X}} = J_X^T\mathbf{F} + \mathbf{G}_0 + J_\theta^T\boldsymbol{\tau}. \tag{C.10}$$

Here,

$$M = diag\,[m_B,\ m_B,\ I_B,\ m_L,\ m_L,\ I_L,\ m_L,\ m_L,\ I_L] \in \mathscr{R}^{9\times 9}, \tag{C.11}$$

$$J_X = \frac{\partial C_C(\mathbf{X})}{\partial \mathbf{X}} \in \mathscr{R}^{8\times 9}, \tag{C.12}$$

$$\mathbf{G}_0 = \mathbf{G}_G + J_e^T\mathbf{F}_e \in \mathscr{R}^9, \tag{C.13}$$

$$\mathbf{G}_G = [0\ \ -m_Bg\ \ 0\ \ 0\ \ -m_Bg\ \ 0\ \ 0\ \ -m_Bg\ \ 0]^T \in \mathscr{R}^9. \tag{C.14}$$

Here, $J_e \in \mathscr{R}^{2\times 9}$ is the CoM Jacobian matrix relating $(\dot{x}_G, \dot{y}_G)$ and $\dot{\mathbf{X}}$.

By differentiating (C.7) twice with respect to time, we obtain

$$J_X\ddot{\mathbf{X}} + \mathbf{C}_0 = \mathbf{0}, \tag{C.15}$$

where

$$\mathbf{C}_0 = \dot{J}_X\cdot\dot{\mathbf{X}}. \tag{C.16}$$

Using (C.10) and (C.15) together, we find the following matrix equation,

$$\begin{bmatrix} M & -J_X^T \\ -J_X & 0 \end{bmatrix}\begin{bmatrix} \ddot{\mathbf{X}} \\ \mathbf{F} \end{bmatrix} = \begin{bmatrix} \mathbf{G}_0 + J_\theta^T\boldsymbol{\tau} \\ \mathbf{C}_0 \end{bmatrix}. \tag{C.17}$$

The matrix on the left-hand-side of the equation has an inverse matrix since M has it. This inverse matrix is given by

$$\begin{bmatrix} M & -J_X^T \\ -J_X & 0 \end{bmatrix}^{-1} = \begin{bmatrix} N_0 & N_1^T \\ N_1 & N_2 \end{bmatrix}. \tag{C.18}$$

Here, $N_0 = M^{-1} - M^{-1}J_X^T(J_XM^{-1}J_X^T)^{-1}J_XM^{-1} \in \mathscr{R}^{9\times 9}$, $N_1 = -(J_XM^{-1}J_X^T)^{-1}J_XM^{-1} \in \mathscr{R}^{8\times 9}$, $N_2 = -(J_XM^{-1}J_X^T)^{-1} \in \mathscr{R}^{8\times 8}$. Then, (C.17) can be solved for $\ddot{\mathbf{X}}$ and $\mathbf{F}$.

$$\begin{bmatrix} \ddot{\mathbf{X}} \\ \mathbf{F} \end{bmatrix} = \begin{bmatrix} N_0 & N_1^T \\ N_1 & N_2 \end{bmatrix}\begin{bmatrix} \mathbf{G}_0 + J_\theta^T\boldsymbol{\tau} \\ \mathbf{C}_0 \end{bmatrix}. \tag{C.19}$$

From (C.2),

$$\boldsymbol{\tau} = J_{\phi 1}^T\tau_\phi \tag{C.20}$$

is satisfied by the virtual work principle and

$$\ddot{\phi} = J_{\phi 2}\ddot{\mathbf{X}} = J_{\phi 2}(N_0(\mathbf{G}_0 + J_\theta^TJ_{\phi 1}^T\tau_\phi) + N_1^T\mathbf{C}_0). \tag{C.21}$$

The dynamics of ϕ is expressed by (5), where

$$M(\theta) = (J_{\phi 2}N_0J_\theta^TJ_{\phi 1}^T)^{-1} \tag{C.22}$$

$$C(\theta, \dot{\theta}) = (J_{\phi 2}N_0J_\theta^TJ_{\phi 1}^T)^{-1}J_{\phi 2}N_1^T\dot{J}_X\dot{\mathbf{X}} \tag{C.23}$$

$$G(\theta, g) = (J_{\phi 2}N_0J_\theta^TJ_{\phi 1}^T)^{-1}J_{\phi 2}N_0\mathbf{G}_G. \tag{C.24}$$

$$\xi(\theta, \mathbf{F}_e) = (J_{\phi 2}N_0J_\theta^TJ_{\phi 1}^T)^{-1}J_{\phi 2}N_0J_e^T\mathbf{F}_e. \tag{C.25}$$

Note that $\mathbf{X}$ is uniquely described by θ, that is, $\mathbf{X} = \mathbf{X}(\theta)$.

Appendix D. CoP position

The relationship between P_{CoP} and τ_ϕ is

$$P_{CoP} = P(\theta)\tau_\phi + Q(\theta, \dot{\theta}) + R(\theta, g). \tag{D.1}$$

Now, we derive Eq. (D.1).

The CoP position P_{CoP} is calculated from the ground reaction forces at the four contact points as follows:

$$P_{CoP} = \frac{F_{RO}}{F_{all}}(x_f + \ell_f) + \frac{F_{RI}}{F_{all}}(x_f - \ell_f) - \frac{F_{LI}}{F_{all}}(x_f - \ell_f) - \frac{F_{LO}}{F_{all}}(x_f + \ell_f), \tag{D.2}$$

where ℓ_f is the length from the ankle joint to the end of the foot, and

$$F_{all} = F_{RO} + F_{RI} + F_{LI} + F_{LO}. \tag{D.3}$$

Each ground reaction force is expressed as follows:

$$F_{LO} = \frac{1}{2}F_y^{LA} + \frac{1}{\ell_f}\tau_{LA}, \tag{D.4}$$

$$F_{LI} = \frac{1}{2}F_y^{LA} - \frac{1}{\ell_f}\tau_{LA}, \tag{D.5}$$

$$F_{RO} = \frac{1}{2}F_y^{RA} + \frac{1}{\ell_f}\tau_{RA}, \tag{D.6}$$

$$F_{RI} = \frac{1}{2}F_y^{RA} - \frac{1}{\ell_f}\tau_{RA}. \tag{D.7}$$

We assume that F_{all} is constant because it corresponds to the total weight. Then, (D.2) can be rewritten as follows:

$$P_{CoP} = J_{Z1}^T\mathbf{F} + J_{Z2}^T\boldsymbol{\tau}, \tag{D.8}$$

$$J_{Z1} = [0 \;\; 0 \;\; 0 \;\; 0 \;\; 0 \;\; -x_f/F_{all} \;\; 0 \;\; x_f/F_{all}]^T, \tag{D.9}$$

$$J_{Z2} = [2/F_{all} \;\; 0 \;\; 0 \;\; -2/F_{all}]^T. \tag{D.10}$$

From (C.19), $\mathbf{F}$ can be expressed as

$$\mathbf{F} = N_1(\mathbf{G}_0 + J_\theta^T\boldsymbol{\tau}) + N_2\mathbf{C}_0. \tag{D.11}$$

Substituting this equation into (D.8), we obtain (D.1), where

$$P(\theta) = (J_{Z1}^T N_1 J_\theta^T + J_{Z2}^T)J_{\phi 1} \tag{D.12}$$

$$Q(\theta, \dot{\theta}) = J_{Z1}^T N_2 \mathbf{C}_0 \tag{D.13}$$

$$R(\theta, g, \mathbf{F}_e) = J_{Z1}^T N_1 \mathbf{G}_0. \tag{D.14}$$

References

[1] Yoneda K, Tamaki T, Ota Y, Kurazume R. Design of bipedal robot with reduced degrees of freedom. J Robot Soc Jpn 2003;21(5):86–93.
[2] Li T, Ceccarelli M. Design and simulated characteristics of a new biped mechanism. Robotica 2015;33:1568–88.
[3] McGeer T. Passive dynamic walking. Int J Rob Res 1990;9(2):62–82.
[4] Collins SH, Ruina A. A bipedal walking robot with efficient and human-like gait. Proceedings of the 2005 IEEE International Conference on Robotics and Automation (ICRA 2005). IEEE; 2005. p. 1983–8.
[5] Braun DJ, Mitchell JE, Goldfarb M. Actuated dynamic walking in a seven-link biped robot. IEEE/ASME Trans Mechatron 2012;17(1):147–56.
[6] Vukobratovic M, Borovac B, Surla D, Stokic D. Biped locomotion: Dynamics, stability, control and application. Springer; 1990.
[7] Al-Shuka HFN, Allmendinger F, Corves B, Zhu W-H. Modeling, Stability and walking pattern generators of biped robots: a review. Robotica 2014;32:907–34.
[8] Nishiwaki K, Kagami S. Simultaneous planning of CoM and ZMP based on the preview control method for online walking control. 2011 11th IEEE-RAS International Conference on Humanoid Robots. IEEE; 2011. p. 745–51.
[9] Dang D, Lamiraux F, Laumond J-P. A framework for manipulation and locomotion with realtime footstep replanning. 2011 11th IEEE-RAS International Conference on Humanoid Robots. IEEE; 2011. p. 676–81.
[10] Alcaraz-Jiménez JJ, Herrero-Pérez D, Martínez-Barberá H. Robust feedback control of ZMP-based gait for humanoid robot Nao. Int J Rob Res 2013.
[11] Luo X, Li W, Zhu C. Planning and control of cop-switch-based planar biped walking. J Bionic Eng 2011;8(1):33–48.
[12] Stephens BJ, Atkeson CG. Dynamic balance force control for compliant humanoid robots. 2010 IEEE/RSJ International Conference on Intelligent Robots and Systems (IROS). IEEE; 2010. p. 1248–55.
[13] Ibanez A, Bidaud P, Padois V. Previewed impedance adaptation to coordinate upper-limb trajectory tracking and postural balance in disturbed conditions. Proc. 16th International Conference on Climbing and Walking Robots and the Support Technologies for Mobile Machines. 2013. p. 519–28.
[14] Beranek R, Fung H, Ahmadi M. A walking stability controller with disturbance rejection based on CMP criterion and ground reaction force feedback. 2011 IEEE/RSJ International Conference on Intelligent Robots and Systems (IROS). IEEE; 2011. p. 2261–6.
[15] Wu N, Tan B-H, Chew C, Poo A-N. Compliant foot system design for bipedal robot walking over uneven terrain. Proc. 16th International Conference on Climbing and Walking Robots and the Support Technologies for Mobile Machines. 2013. p. 383–91.
[16] Kajita S, Morisawa M, Miura K, Nakaoka S, Harada K, Kaneko K, et al. Biped walking stabilization based on linear inverted pendulum tracking. 2010 IEEE/RSJ International Conference on Intelligent Robots and Systems (IROS). IEEE; 2010. p. 4489–96.
[17] Aoyama T, Hasegawa Y, Sekiyama K, Fukuda T. Stabilizing and direction control of efficient 3-D biped walking based on PDAC. IEEE/ASME Trans Mechatron 2009;14(6):712–8.
[18] Geng T, Gan JQ. Planar biped walking with an equilibrium point controller and state machines. IEEE/ASME Trans Mechatron 2010;15(2):253–60.
[19] Sugihara T. Consistent biped step control with COM-ZMP oscillation based on successive phase estimation in dynamics morphing. 2010 IEEE International Conference on Robotics and Automation. IEEE; 2010. p. 4224–9.
[20] Ito S, Nakazawa A, Onozawa T, Nishio S, Sasaki M. Hip joint structure for biped robot with reduced DoF's of motion. Proc. 16th International Conference on Climbing and Walking Robots and the Support Technologies for Mobile Machines. 2013. p. 529–36.
[21] Ito S, Kawasaki H. Regularity in an environment produces an internal torque pattern for biped balance control. Biol Cybern 2005;92(4):241–51.
[22] Ito S, Nishio S, Fukumoto Y, Sasaki M. Biped balance control based on the feedback of ground reaction forces with gravity compensation. Proceedings of ISCIE/ASME 2014 International Symposium on Flexible Automation. 2014. ISFA2014–16L.
[23] Goswami A. Postural stability of biped robots and the foot-rotation indicator (FRI) Point. Int J Rob Res 1999;18(6):523.
[24] Ito S, Sasaki M. Motion control of biped lateral stepping based on zero moment point feedback for adaptation to slopes. Intech; 2011. p. 15–34. chapter 2.
[25] Hyon S-H, Cheng G. Gravity compensation and full-body balancing for humanoid robots. 2006 6th IEEE-RAS International Conference on Humanoid Robots. IEEE; 2006. p. 214–21.
[26] Jianghai Z, Xiaojian Z, Cheng T. Gait planning of biped robot based on feed-forward compensation of gravity moment. 2015 IEEE International Conference on Mechatronics and Automation (ICMA). IEEE; 2015. p. 1181–6.
[27] Ito S, Nishio S, Fukumoto Y, Matsushita K, Minoru S. Gravity compensation and feedback of ground reaction forces for biped balance control. Appl Bionics Biomech 2017;23(4):742–7.